



SPECIAL ISSUE PAPER

# 3-D cell-level chlorophyll fluorescence imaging of ozone-injured sunflower leaves using a new passive light microscope system

Ryosuke Endo<sup>1,\*</sup> and Kenji Omasa<sup>2</sup>

<sup>1</sup> Advanced Research Institute for the Sciences and Humanities, Nihon University, 6F Ichigaya Tokyu Building, 4-2-1 Kudan-kita, Chiyoda, Tokyo 102-0073, Japan

<sup>2</sup> Department of Biological and Environmental Engineering, Graduate School of Agricultural and Life Sciences, The University of Tokyo, 1-1-1 Yayoi, Bunkyo, Tokyo 113-8657, Japan

Received 8 May 2006; Accepted 13 September 2006

## Abstract

**A passive light microscope system has been developed, capable of reconstructing an extended-focus 3-D cell-level image of chlorophyll fluorescence and  $\Phi_{PSII}$  of intact attached leaves using a limited number of focal plane images of chlorophyll fluorescence. Using this system, the relationships between the depth of the mesophyll cells in spongy tissue and the intensity of the chlorophyll fluorescence and the  $\Phi_{PSII}$  were investigated in sunflower leaves exposed to 300 ppb ozone for 12 h at a PPFD of  $300 \mu\text{mol m}^{-2} \text{s}^{-1}$  actinic light. After ozone exposure, fluorescence intensity ( $F$ ) largely decreased in the cells just under the epidermal cells (within  $\sim 20 \mu\text{m}$  of the epidermal cells), but the sites where fluorescence intensity decreased had no relationship to the position of the stomata. By contrast, the distribution of  $\Phi_{PSII}$  showed no change after the ozone exposure. These findings suggest that ozone-induced inhibition occurs in the cells just under the epidermal cells by reducing the light absorption of the chloroplasts, while the operating quantum efficiency of PSII photochemistry is maintained.**

Key words: Chlorophyll fluorescence, 3-D imaging, microscope, ozone.

## Introduction

Tropospheric ozone is one of the worst global air pollutants, causing serious vegetative damage and forest

decline (Yunus and Iqbal, 1996; Sandermann *et al.*, 1997). Half of forests in the world are predicted to be exposed to phytotoxic ozone levels by 2100 (Fowler *et al.*, 1999). Stratospheric ozone is decreasing due to ozone destruction by human-made chlorofluorocarbons and  $\text{NO}_x$ , whereas the concentration of ozone at ground level appears to be stable or increasing in many industrialized countries (Oltmans *et al.*, 1998; Akimoto, 2003). Increases in the surface ozone concentration are largely caused by photochemical oxidant pollution produced in the atmosphere by complex photochemical reactions involving  $\text{NO}_x$  and hydrocarbons (Lelieveld and Crutzen, 1990; Oltmans *et al.*, 1998).

Ozone damage in plants has been investigated with regard to its oxidizing potential and the consequential formation of radicals and reactive oxygen species, such as the superoxide radical, hydrogen peroxide, and hydroxyl radical (Heath, 1980, 1987). These radicals and reactive oxygen species attack the plasma membrane, causing an increase in oxidative stress within the cells (Heath, 1994; Schraudner *et al.*, 1997; Omasa *et al.*, 2002) and, consequently, decreasing the plants' physiological and biochemical activities. Because intercellular ozone concentrations have been reported to be approximately zero under high ozone exposure (Laisk *et al.*, 1989; Omasa *et al.*, 2000, 2002), ozone itself is unlikely to enter plant cells.

Plant productivity decreases due to ozone inhibition of photosynthesis. This inhibition can be the result of changes in stomatal conductance or photosynthetic enzymatic activities (Pell *et al.*, 1992). Changes in stomatal conductance may be associated with changes in the plasmalemmae of guard cells (Castillo and Heath, 1990;

\* To whom correspondence should be addressed. E-mail: ryosuke-endo@arish.nihon-u.ac.jp

Torsethaugen *et al.*, 1999), and changes in photosynthetic enzymatic activities may be due to the effect of oxygen radicals generated by ozone. However, it is unclear whether these are the main factors involved in the decline of photosynthesis after ozone exposure.

The distribution of ozone-injured sites varies all over the leaf, and the degree of injury is seldom uniform (Omasa *et al.*, 1981). Therefore, specifying the effects of ozone on photosynthetic activity requires a spatial measuring method. Chlorophyll fluorescence imaging is one of the most effective methods for analysing photosynthetic activity in *in situ* plant leaves (Omasa *et al.*, 1987; Daley *et al.*, 1989; Lichtenthaler and Miehe, 1997). Recently, microscopic fluorescence imaging systems have been developed for cellular- and chloroplast-level analyses (Oxborough and Baker, 1997; Küpper *et al.*, 2000; Leipner *et al.*, 2001; Lawson *et al.*, 2002; Endo and Omasa, 2004). Using a chlorophyll fluorescence imaging system, Leipner *et al.* (2001) identified the primary sites of ozone-induced perturbation in *Phaseolus vulgaris*. By using a 680 nm bandpass filter and a 695 nm longpass filter, chlorophyll fluorescence from the upper mesophyll cell layer in a leaf was differentiated from fluorescence below the leaf surface. Ozone-injured sites were not related to the location of stomata, and a greater number of injured sites was identified over the 695 nm images than in the 680 nm images (Leipner *et al.*, 2001). This method showed a difference of inhibition in depth, based on the fact that fluorescence at 680 nm is strongly absorbed by chlorophylls within the overlying cells compared with 695 nm, although it does not allow direct measurement of the depth of the cells in the leaves.

High-resolution imaging with a microscope causes the inevitable problem of the limited depth of the observable field. Because a leaf surface tends to be uneven, not much of a captured image is in focus, and inaccurate photosynthetic parameters can be generated from fluorescence images that include areas that are out of focus. This problem can be solved by reconstructing an extended-focus image from a series of images captured at different focal planes (shape from focus). This method provides not only an extended-focus image but also a 3-D image; therefore, the direct relationship between the photosynthetic parameter and depth of the cells in the leaves can be analysed.

Many methods have been developed to extract focal points from each pixel in multifocal plane images (Nayar and Nakagawa, 1994; Russ, 1998; Omasa, 2000). To apply this technique to fluorescence imaging, a method that does not alter the intensity of each pixel before and after processing is required, because fluorescence intensities of pixels in the images will be used to calculate the photosynthetic parameters. The shape-from-focus method is the most effective for extracting the focal point from focal plane images. Using this method, Rolfe and Scholes (2002) captured an extended-focus image of chlorophyll

fluorescence from intact leaves from a total of 39 images at 5.5  $\mu\text{m}$  intervals using a  $\times 10$  objective lens. Using this system, however, it took a long time to acquire a series of images at different focal depths. This problem can cause inaccurate 3-D reconstruction because of sample movement, especially at high magnification. Therefore, an alternative reconstruction method capable of extracting an accurate focal point from fewer focal plane images is required.

Omasa (2000) has developed a modified shape-from-focus algorithm that was based on a linear regression (LR) operator. This method is characterized by making an extended-focus image from fewer focal plane images by interpolating the distance between the captured images. In addition, it was found that this method was effective for reconstructing range images from monocular light microscope images of plant cells (Omasa, 2000). However, this method was applied only to a reflected light image, and was not applied to a chlorophyll fluorescence image. Therefore, 3-D analysis of photosynthetic activity in *in situ* plant leaves by this method, has not been investigated.

In this study, the method based on the LR operator was applied to produce microscopic extended-focus images of the chlorophyll fluorescence of ozone-injured leaves, and they were used to clarify the relationship between the depth from the leaf surface and the injured site in an *in situ* sunflower leaf. This system was also designed to reconstruct 3-D chlorophyll fluorescence and  $\Phi_{\text{PSII}}$  images.

## Materials and methods

### Growth conditions

Sunflower (*Helianthus annuus* L. cv. 'Sun Hope') seeds were sown in a growth chamber in pots filled with artificial soil (mixture of vermiculite, perlite, 1:1 v/v). The plants were illuminated for 12 h each day with fluorescent lights ( $PPFD$   $300 \mu\text{mol m}^{-2} \text{s}^{-1}$  at plant height). The air temperature was 26.5 °C during the day and 20 °C at night. The relative humidity was 45% during the day and 60% at night. Plants were watered daily with a nutrient solution (1:1000 dilution of HYPONeX 5-10-5, HYPONeX Japan, Osaka, Japan). The plants were grown for 4 weeks, and fully expanded mature leaves were used *in situ* for the experiments.

### Ozone treatment

At 4 weeks, the plants were transferred to another environmentally controlled chamber (illuminated with fluorescent lights at  $PPFD$   $300 \mu\text{mol m}^{-2} \text{s}^{-1}$ ) and exposed to air containing a 300 ppb ozone concentration for 12 h. Ozone was generated using an ozone generator (OES-10A, Dylec Inc., Osaka, Japan) and mixed with the inlet air entering the chamber. The ozone concentration inside the chamber was continuously monitored using an ozone monitor (Model 1200, Dylec Inc.). After ozone exposure, the treated plants were transferred immediately to the 3-D chlorophyll fluorescence imaging system.

### Chlorophyll fluorescence imaging system

Chlorophyll fluorescence images were captured with a computerized light microscope system, which was described in Endo and Omasa

(2004). The system comprised a modified light microscope with a  $\times 20$  objective lens (BD Plan Apo 20, N.A.=0.42; Mitutoyo), a stepping-motor control system for controlling each axis of the microscope stage and lens barrel, a cooled charge-coupled device (CCD) camera (Cascade, Photometrix), and a personal computer for deconvoluting the series of focal plane images and analysing the resulting 3-D images and fluorescence parameter images. The stepping motor system is connected to the computer and is able to move the lens barrel precisely to acquire each focal plane image at a constant 2-axis interval. The images, captured at 653 horizontal $\times$ 492 vertical pixels per frame with 16-bit resolution, were recorded on a hard disk and analysed using software developed with Visual Basic (Version 6.0, Microsoft, Seattle, WA, USA) and commercial software (Erdas Imagine Version 8.4, Erdas).

During the experiment, continuous actinic light at a  $PPFD$  of  $300 \mu\text{mol m}^{-2} \text{s}^{-1}$  for photosynthesis and a saturation light pulse at a  $PPFD$  of  $3800 \mu\text{mol m}^{-2} \text{s}^{-1}$  to cause transient saturation of photochemistry were provided by 180 W metal halide lamps (LS-M180, Sumita Optical Glass Inc.) equipped with short-pass filters (model 4-96,  $\lambda \leq 620 \text{ nm}$ ; Corning, USA); the light was passed through heat-absorbing filters via an optical fibre system and was controlled by electric shutters (Shutter Controller, EMS). Chlorophyll fluorescence excited by these lights was imaged by the CCD camera through an optical filter (model 2-64, wavelength  $\lambda \geq 640 \text{ nm}$ ; Corning) in the lens barrel of the microscope.

After ozone exposure for 12 h, the plants were moved to the microscopic imaging system stage. After a 20 min adaptation period under continuous actinic light for photosynthesis ( $PPFD$   $300 \mu\text{mol m}^{-2} \text{s}^{-1}$ ), the fluorescence intensity image ( $F$ ) from the abaxial side of the sunflower leaf was captured. Just after this measurement, a fluorescence intensity image ( $F'_m$ ) was measured during a 1.2 s light pulse ( $PPFD$  of  $3800 \mu\text{mol m}^{-2} \text{s}^{-1}$ ) to cause saturation of photochemistry. To reconstruct a 3-D extended-focus image, a series of unprocessed  $F$  and  $F'_m$  images was captured at different focal planes for every additional  $4 \mu\text{m}$  from a reference  $z$  point. Because irradiation of a saturation pulse at short intervals can alter the photochemistry of leaves, there was a 30 s period before capturing the next set of  $F$  and  $F'_m$  images after the focal plane was moved. In total, 15 sets of  $F$  and  $F'_m$  images we captured.

### Image deconvolution

A linear regression (LR) operator was used to reconstruct extended-focus 3-D images from a series of limited focal plane images, which were captured by  $z$ -axis traversal of the lens barrel (Omasa, 2000). Figure 1 shows the procedure for producing an image deconvolution. For all pixels in all unprocessed images, the focus measure values were calculated automatically using software we developed with Visual Basic (Version 6.0, Microsoft).

The LR operator, which is effective for determining the focus measure, was used to obtain extended-focus images from a series of unprocessed images at different focal planes. The data on each axis of the four square-line masks were calculated:  $M_k(i, j)$ , where  $k=1, 2, 3, 4$ , and  $(i, j)$  indicates the centre of the  $M_s \times M_s$  line mask (Fig. 1). Focus measure  $f(i, j)$  can subsequently be determined using the LR operator, in which the sum of the absolute error between intensity  $I(i, j)$  and the regression line of  $I(i, j)$  is calculated using the least-squares method on the axes ( $p_k, k=1, 2, 3, 4$ ) of each mask:

$$f(i, j) = \sum_{k=1,2,3,4} \sum_{x,y \in M_k(i,j)} |I(x, y) - [a_k(i, j) + b(i, j)p_k(i, j)]| \quad (1)$$

where  $a_k(i, j)$  and  $b_k(i, j)$  represent the regression coefficients on line mask  $M_k(i, j)$  in which  $x, y \in M_k(i, j)$  indicates that  $(x, y)$  exists in  $M_k(i, j)$ .

The number of focal plane images was limited to 15 to shorten the measuring time. Despite having used a discrete range of depth,

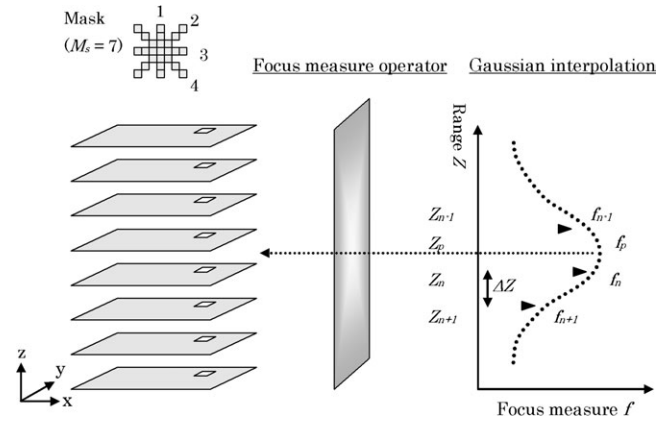


**Fig. 1.** The sequence of modified shape-from-focus images used in the algorithm for 3-D reconstruction of the chlorophyll fluorescence images.

the application of Gaussian interpolation provided smoother, more accurate range estimates (Fig. 1). The focus measure data at each pixel  $(i, j)$  in the images of continuous focal planes have a Gaussian distribution, where the optimum focus point, the focal range  $z_p(i, j)$ , is the peak of the Gaussian distribution. This assumption allows  $z_p(i, j)$  to be determined from three focus measures ( $f_{n-1}, f_n, f_{n+1}$ ) and the distance between neighbouring focal planes ( $\Delta z$ ):

$$z_p = \frac{(\ln f_n - \ln f_{n+1})(z_n^2 - z_{n-1}^2) - (\ln f_n - \ln f_{n-1})(z_n^2 - z_{n+1}^2)}{2\Delta z [(\ln f_n - \ln f_{n-1}) + (\ln f_n - \ln f_{n+1})]} \quad (2)$$

where  $f_n$  is the largest value in a series of focus measures at the pixel level estimated using equation (1) and coordinates  $(i, j)$  are omitted for simplicity. The 3-D image estimated by equation (2) included some spike-like noise, which was removed using a median filter.

An extended-focus image was generated by interpolating the original chlorophyll fluorescence intensities using the information on the focus range at each pixel. Intensity  $I_p(i, j)$  focused at  $(i, j)$  was estimated by

$$I_p = I_{n-1} \frac{z_n - z_p}{\Delta z} + I_n \frac{z_p - z_{n-1}}{\Delta z} \quad (3)$$

where  $I_n$  and  $I_{n-1}$  are the fluorescence intensities at pixel  $(i, j)$  in the image captured at  $z_n$  and  $z_{n-1}$ , respectively, and coordinates  $(i, j)$  are omitted for simplicity.

### Calculation of $\Phi_{PSII}$

To convert an intensity image into a yield image, each intensity image ( $F$  and  $F'_m$ ) was divided by the average value of fluorescence emitted from a fluorescent standard card induced by the corresponding light intensity. Because the fluorescent card has a constant fluorescent yield regardless of light intensity, this process enabled us to convert intensity images to yield images. The  $\Phi_{PSII}$  was calculated using the following equation (Genty *et al.*, 1989):

$$\Phi_{PSII} = \frac{\left(\frac{F'_m}{R_{SL}}\right) - \left(\frac{F}{R_{AL}}\right)}{\left(\frac{F'_m}{R_{SL}}\right)} \quad (4)$$

where  $R_{SL}$  and  $R_{AL}$  are the values of the fluorescence emitted from the fluorescent standard card induced by the saturation light pulse and the actinic light, respectively. The  $\Phi_{PSII}$  image represents the yield of linear electron transport through PSII, with pixel values



ranging from 0 to 1 (Genty *et al.*, 1989; Maxwell and Johnson, 2000).

## Results

Figure 2 shows a series of unprocessed  $F$  images captured at different focal planes before ozone exposure. The plane of focus in the first image was located close to the abaxial leaf surface. At a 30 s interval after each 4  $\mu\text{m}$  movement of the focal plane in the direction of the adaxial surface, the following image was captured, and this process was repeated 14 times. As can be seen in Fig. 2, each image has an area in focus and an area out of focus, and each shows the meshed structure indicative of the cells of spongy tissue. Each image clearly showed that the sample had non-uniform fluorescent intensity.

From these images, the fluorescence intensity of each focal point in the field of view was calculated using equations (1) to (3), and extended-focus images of  $F$  and  $F'_m$  were produced. Extended-focus 3-D images of  $F$  and

$F'_m$  were reconstructed by overlaying the 3-D range image with the extended-focus image. The resulting 3-D range image was the smoothest and the most exact when the mask size for the LR operation was  $M_s=11$  and that for the median filter was  $M_s=5$ . The  $\Phi_{\text{PSII}}$  image was calculated from extended-focus images of  $F$  and  $F'_m$  by equations (4), and 3-D  $\Phi_{\text{PSII}}$  was reconstructed in the same way.

An extended-focus 3-D image of chlorophyll fluorescence ( $F$ ) at steady-state at a  $PPFD$  of  $300 \mu\text{mol m}^{-2} \text{s}^{-1}$  actinic light before ozone exposure is shown in Fig. 3. The relationship between the distance from the first focal plane depth (Fig. 2A) and fluorescence intensity at the pixels on the  $X-X'$  line (Fig. 3B) is shown in Fig. 3C. Before ozone exposure, the fluorescence intensity was non-uniformly distributed in the mesophyll areas and had no relationship to the depth in the leaf (Fig. 3C).

An extended-focus 3-D image of  $\Phi_{\text{PSII}}$  at a  $PPFD$  of  $300 \mu\text{mol m}^{-2} \text{s}^{-1}$  actinic light before ozone exposure was constructed from the images of  $F$  and  $F'_m$  (Fig. 4A). In contrast to the chlorophyll fluorescence, the  $\Phi_{\text{PSII}}$  values were uniformly distributed across the leaf area. The relationship between the distance from first focal plane and the  $\Phi_{\text{PSII}}$  values at the pixels on the  $X-X'$  line (Fig. 3B) are shown in Fig. 4B. The  $\Phi_{\text{PSII}}$  values on the  $X-X'$  line (range, 0.43–0.51) had no relationship to the depth in the leaf.

An extended-focus 3-D image of fluorescence intensity ( $F$ ) at steady-state after exposure to 300 ppb ozone for 12 h are shown in Fig. 5. After ozone exposure, areas of high-intensity and low-intensity chlorophyll fluorescence were recognized. The relationship between the distance from the first focal plane and the fluorescence intensity along the  $X-X'$  line (Fig. 5B) is shown in Fig. 5C. Fluorescence intensity was low near the abaxial leaf surface and showed higher values deeper within the leaf. Fluorescence intensities from cells approximately 40  $\mu\text{m}$  below the abaxial leaf surface were almost the same as the mean fluorescence intensity of the leaf before ozone exposure.

An extended-focus 3-D image of  $\Phi_{\text{PSII}}$  after exposure to 300 ppb ozone was constructed from the images of  $F$  and  $F'_m$  (Fig. 6A). In contrast to the chlorophyll fluorescence values, the  $\Phi_{\text{PSII}}$  values were uniformly distributed across the leaf area, despite the  $\Phi_{\text{PSII}}$  values having greater variability than before ozone exposure. The relationship between the distance from the first focal plane and the  $\Phi_{\text{PSII}}$  values at the pixels on the  $X-X'$  line (Fig. 5B) are shown in Fig. 6B. The  $\Phi_{\text{PSII}}$  values on  $X-X'$  line (range, 0.39–0.52) had no significant relationship to the depth of the cells in the leaf, although only a slight tendency for the  $\Phi_{\text{PSII}}$  values to decrease closer to the abaxial leaf surface was found.

Figure 7A shows the reflection image in the same area of the ozone-exposed leaf as shown in Fig. 5B. The

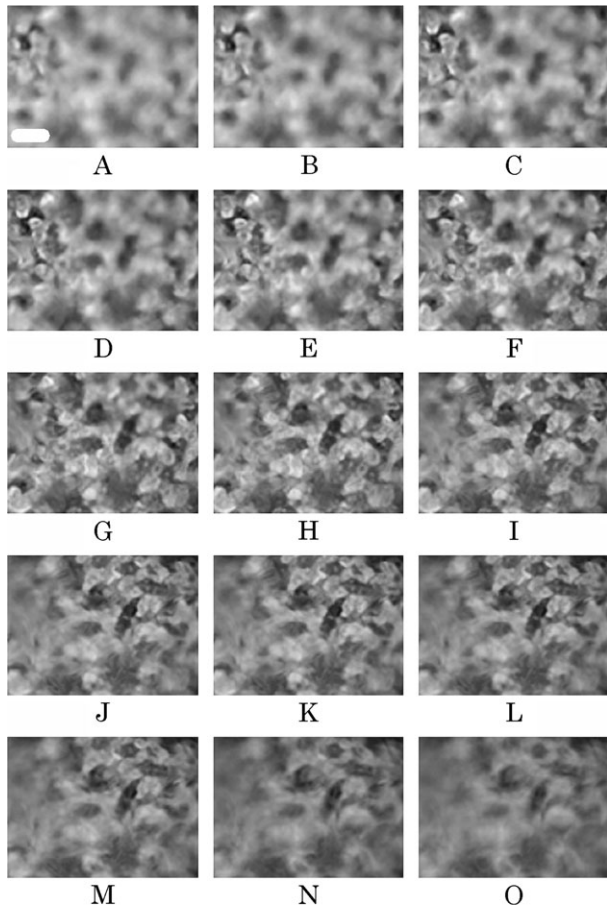


**Fig. 2.** A series of unprocessed chlorophyll fluorescence ( $F$ ) images captured from the abaxial side of a sunflower leaf at steady-state under an actinic light of  $300 \mu\text{mol m}^{-2} \text{s}^{-1}$ . Images were captured across 15 focal planes at 4  $\mu\text{m}$  intervals using a  $\times 20$  objective lens. Scale bar=40  $\mu\text{m}$ .

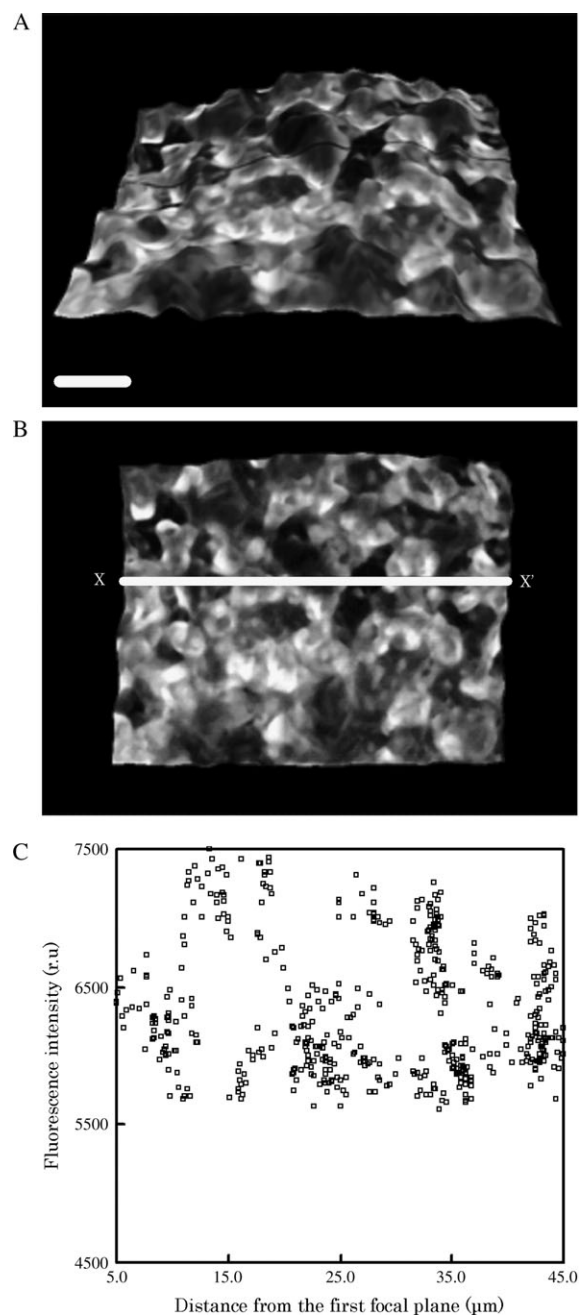


**Fig. 3.** 3-D extended-focus chlorophyll fluorescence ( $F$ ) images of mesophyll cells in the spongy tissue of a sunflower leaf before ozone exposure, calculated using the linear regression (LR) operator described in the text and Gaussian interpolation. (A) Image of the abaxial leaf surface viewed at  $45^\circ$  from the horizontal. (B) Image of the leaf surface viewed from directly above. (C) The relationship between distance from the first focal plane (Fig. 2A) and fluorescence intensity ( $n=623$  points). The X-X' line in (B) is the profile analysis line used for the plot in (C). Scale bar= $40\ \mu\text{m}$ .

dashed white circle indicates a stoma. As can be seen in Fig. 7B, there was no relationship between the site where fluorescence intensity decreased strongly (dashed black line) and the position of the stoma.

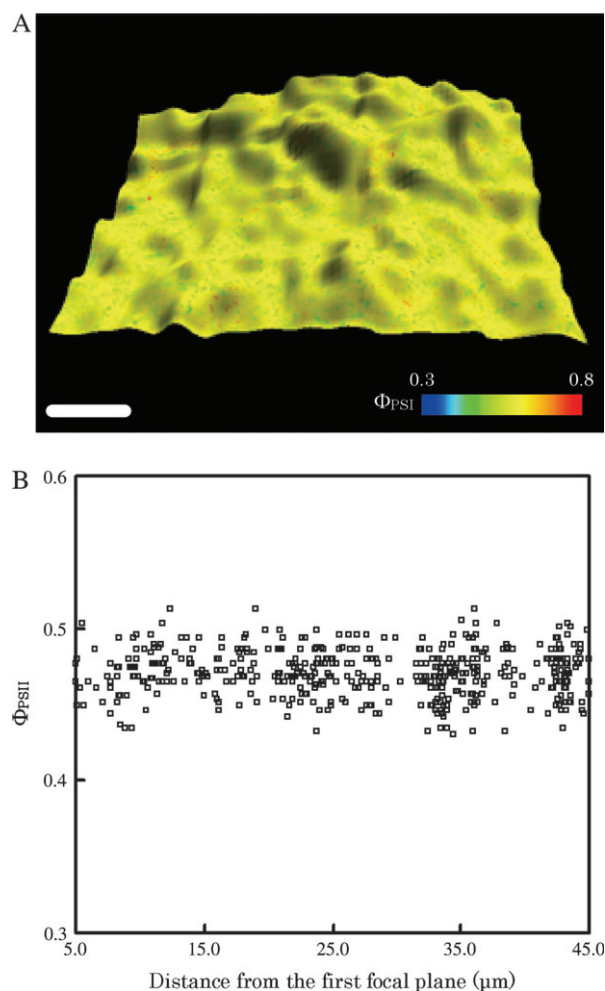


**Fig. 4.** 3-D extended-focus  $\Phi_{\text{PSII}}$  images of the mesophyll cells shown in Fig. 3. (A) The 3-D extended-focus  $\Phi_{\text{PSII}}$  image. (B) The relationship between distance from the first focal plane and  $\Phi_{\text{PSII}}$ . The  $\Phi_{\text{PSII}}$  images were calculated from two kinds of fluorescence intensity images:  $F$  was taken at a  $PPFD$  of  $300\ \mu\text{mol m}^{-2}\ \text{s}^{-1}$  actinic light and  $F'_m$  was taken during a saturating light pulse of  $3800\ \mu\text{mol m}^{-2}\ \text{s}^{-1}$ . The 623 points plotted were taken along the centre line in (B). Scale bar= $40\ \mu\text{m}$ .

## Discussion

A new passive light microscope system was developed that is capable of reconstructing 3-D cell-level images of  $F$ ,  $F'_m$ , and  $\Phi_{\text{PSII}}$  of intact attached leaves from a limited number of unprocessed images of chlorophyll fluorescence at different focal planes. The relationships between the depth of mesophyll cells in spongy tissue and chlorophyll fluorescence parameters ( $F$  and  $\Phi_{\text{PSII}}$ ) were investigated in sunflower leaves exposed to 300 ppb ozone for 12 h at a  $PPFD$  of  $300\ \mu\text{mol m}^{-2}\ \text{s}^{-1}$  actinic light.

In chlorophyll fluorescence imaging, 680 nm band-pass and 695 nm long-pass filters have been used to estimate the distance of cells from the leaf surface (Leipner *et al.*, 2001). Fluorescence at 680 nm is strongly absorbed by chlorophylls compared with that over 695 nm. Therefore,

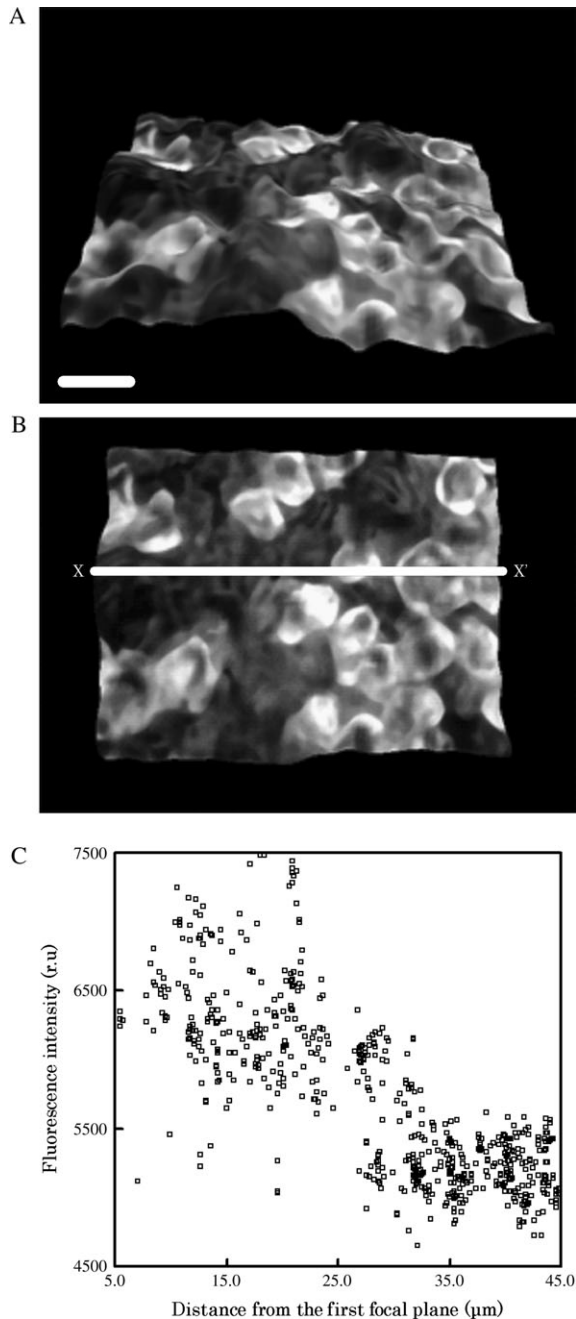


**Fig. 5.** 3-D extended-focus chlorophyll fluorescence ( $F$ ) images of mesophyll cells in the same sunflower leaf after 300 ppb ozone exposure for 12 h. (A) The leaf surface viewed at  $45^\circ$  from the horizontal. (B) The surface viewed from directly above. (C) The relationship between distance from the first focal plane and fluorescence intensity ( $n=623$  points). The  $X-X'$  line in (B) is the profile analysis line used for the plot in panel (C). Scale bar= $40\ \mu\text{m}$ .

the fluorescence at 680 nm is attributed to reflection of the fluorescence from chloroplasts in cell layers near to the leaf surface. By contrast, the fluorescence over 695 nm reflects that from deeper cell layers, because the fluorescence over 695 nm is not absorbed as much as that at 680 nm. However, cells without overlying cells are not

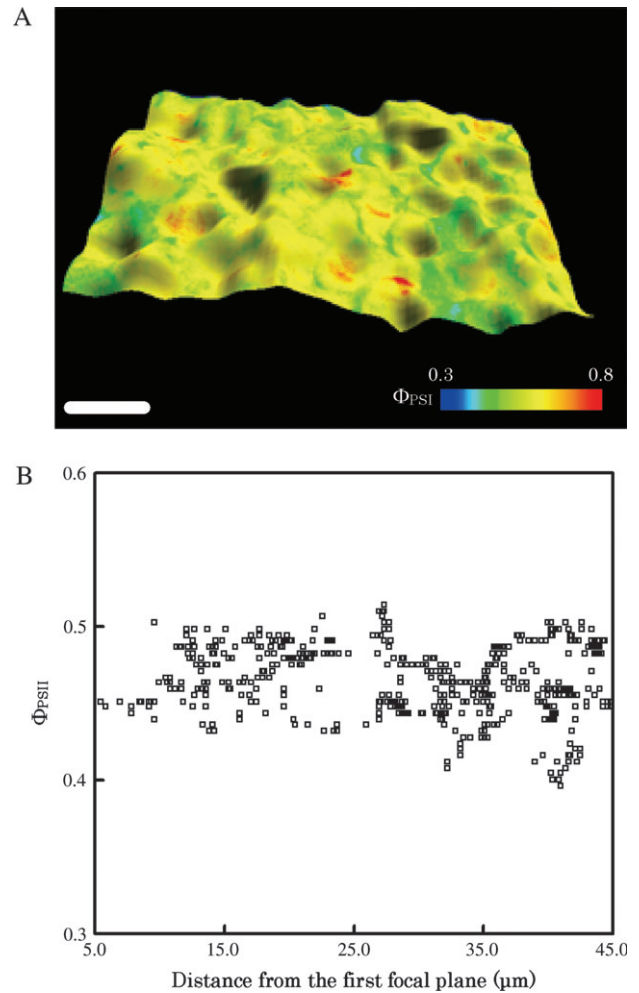


**Fig. 6.** (A) 3-D extended-focus  $\Phi_{\text{PSII}}$  image of mesophyll cells shown in Fig. 5. (B) The relationship between distance from the first focal plane and  $\Phi_{\text{PSII}}$ .  $\Phi_{\text{PSII}}$  images were calculated from two kinds of fluorescence intensity images:  $F$  was taken at a  $PPFD$  of  $300\ \mu\text{mol m}^{-2}\ \text{s}^{-1}$  actinic light and  $F'_m$  was taken during a saturating light pulse of  $3800\ \mu\text{mol m}^{-2}\ \text{s}^{-1}$ . The 623 points plotted were taken along the centre line in (B). Scale bar= $40\ \mu\text{m}$ .

always located near the abaxial leaf surface. In cancellous structures such as spongy tissue, for example, the fluorescence from internal cells may be not absorbed as expected. The 3-D images reconstructed from a series of focal plane images permit the position of internal cells to be estimated more directly.

Before ozone exposure, the chlorophyll fluorescence values were non-uniformly distributed over the field of view. If this result is attributed to the cells being found at depths where chlorophyll fluorescence was not detected, the  $\Phi_{\text{PSII}}$  value would be zero. However, as the  $\Phi_{\text{PSII}}$  value of the extended-focus 3-D images were uniform at 0.43–0.51 (Fig. 4B), the non-uniform distribution of chlorophyll fluorescence was due to variability in chlorophyll fluorescence intensity of the chloroplasts into the cells. The uniform distribution of the  $\Phi_{\text{PSII}}$  values indicates



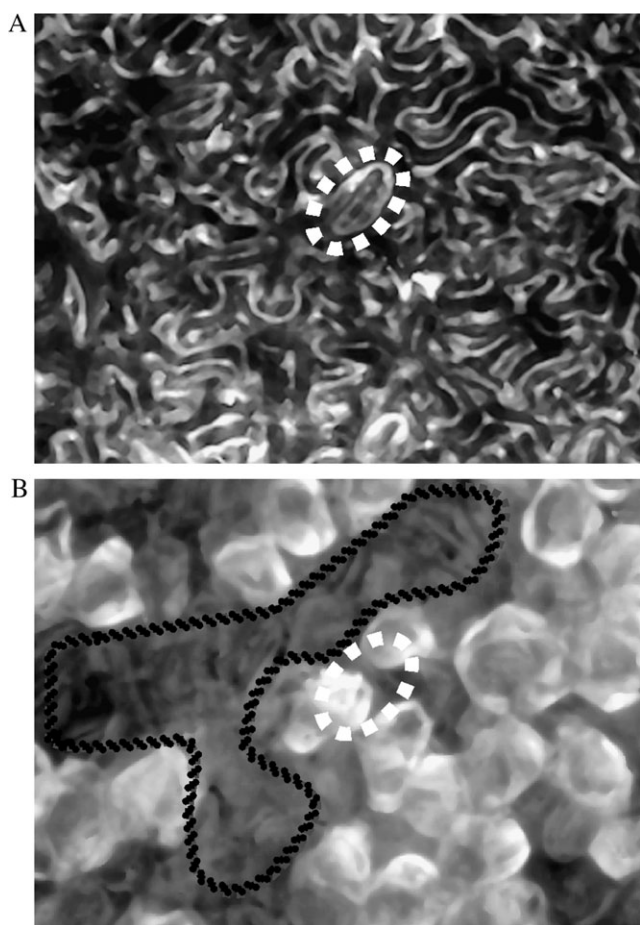


**Fig. 7.** (A) Reflection image and (B) fluorescence intensity ( $F$ ) image of the mesophyll cells shown in Fig. 5. The dashed white circles lines in (A) and (B) represent the position of a stomate confirmed from the reflection image. The black dotted line in (B) encloses an area in which fluorescence intensity decreased strongly. Scale bar=40  $\mu\text{m}$ .

that, within the field of view, each chloroplast has the same quantum efficiency of electron flux through PSII photochemistry.

The change in the distribution of chlorophyll fluorescence after exposure to 300 ppb ozone indicated the inhibition of photosynthesis that had been caused. Furthermore, the sites where the fluorescence intensity decreased were located close to the abaxial leaf surface and were not related to the positions of the stoma, a finding also reported by Leipner *et al.* (2001). Such a phenomenon may occur as a result of ozone diffusion through gaps in the cuticle, or ozone may diffuse rapidly once entering the spongy tissue via open stomata through the air spaces. Ozone exposure appears to increase the vulnerability of the mesophyll cells within sunflower leaves, and the function of the chloroplasts subsequently decreases due to light irradiation. Based on the fluorescence images, decreases in chlorophyll fluorescence were not seen in chloroplast units but were observed at the single cell level, indicating that ozone first attacks mesophyll cells and then

the function of the chloroplasts in the injured cell is reduced. This would be consistent with the dysfunction of guard-cell plasmalemmae caused by ozone invasion (Castillo and Heath, 1990; Torsethaugen *et al.*, 1999).

No relationship was found between  $\Phi_{\text{PSII}}$  value and the depth of cells below the leaf surface. This result indicates that ozone invasion of the leaf caused a decrease in fluorescence intensity in the perturbed cells, but it did not cause a decrease in the quantum efficiency of electron flux through PSII at steady-state.

In summary, the passive light microscope system developed for this study allowed us to quantify the depth of cells in spongy tissue based on reconstructed 3-D images. Our findings indicate the importance of distance from the leaf surface with regard to ozone-injury. This 3-D imaging system can thus be a very effective tool for analysing the photosynthetic activity of uneven leaf cells, especially when focus depth is restricted by the use of a high-magnification lens.

### Acknowledgements

We thank K Takayama (Ehime University) and A Konishi (The University of Tokyo) for helpful discussions and comments on the manuscript. This study was funded by the Japan Society for the Promotion of Science (no. 03J11319).

### References

- Akimoto H. 2003. Global air quality and pollution. *Science* **302**, 1716–1719.
- Castillo FJ, Heath RL. 1990.  $\text{Ca}^{2+}$  transport in membrane vesicles from pinto bean leaves and its alteration after ozone exposure. *Plant Physiology* **94**, 788–795.
- Daley PF, Raschke K, Ball JT, Berry JA. 1989. Topography of photosynthetic activity of leaves obtained from video images of chlorophyll fluorescence. *Plant Physiology* **90**, 1233–1238.
- Endo R, Omasa K. 2004. Chlorophyll fluorescence imaging of individual algal cells: effects of herbicide on *Spirogyra distenta* at different growth stages. *Environmental Science and Technology* **38**, 4165–4168.
- Fowler D, Cape JN, Coyle M, Flechard C, Kuylensstierna J, Hicks K, Derwent D, Johnson C, Stevenson D. 1999. The global exposure of forest ecosystems to air pollutants. *Water, Air, and Soil Pollution* **116**, 5–32.
- Genty B, Briantais JM, Baker NR. 1989. The relationship between the quantum yield of photosynthetic electron-transport and quenching of chlorophyll fluorescence. *Biochimica et Biophysica Acta* **990**, 87–92.
- Heath RL. 1980. Initial events in injury to plants by air pollutants. *Annual Review of Plant Physiology* **31**, 395–431.
- Heath RL. 1987. The biochemistry of ozone attack on plasma membrane of plant cells. *Recent Advances in Phytochemistry* **21**, 29–54.
- Heath RL. 1994. Possible mechanisms for inhibition of photosynthesis by ozone. *Photosynthesis Research* **39**, 439–451.
- Küpper H, Šetlík I, Trtílek M, Nedbal L. 2000. A microscope for two-dimensional measurements of *in vivo* chlorophyll fluorescence

- kinetics using pulsed measuring radiation, continuous actinic radiation, and saturating flashes. *Photosynthetica* **38**, 553–570.
- Laisk A, Kull O, Moldau H.** 1989. Ozone concentration in leaf intercellular air space is close to zero. *Plant Physiology* **90**, 1163–1167.
- Lawson T, Oxborough K, Morison JIL, Baker NR.** 2002. Responses of photosynthetic electron transport in stomatal guard cells and mesophyll cells in intact leaves to light, CO<sub>2</sub>, and humidity. *Plant Physiology* **128**, 52–62.
- Lelieveld J, Crutzen PJ.** 1990. Influences of cloud photochemical processes on tropospheric ozone. *Nature* **343**, 227–232.
- Leipner J, Oxborough K, Baker NR.** 2001. Primary sites of ozone-induced perturbations of photosynthesis in leaves: identification and characterization in *Phaseolus vulgaris* using high resolution chlorophyll fluorescence imaging. *Journal of Experimental Botany* **52**, 1689–1696.
- Lichtenthaler HK, Miehe JA.** 1997. Fluorescence imaging as a diagnostic tool for plant stress. *Trends in Plant Science* **2**, 316–320.
- Maxwell K, Johnson GN.** 2000. Chlorophyll fluorescence: a practical guide. *Journal of Experimental Botany* **51**, 659–668.
- Nayar SK, Nakagawa Y.** 1994. Shape from focus. *IEEE Transactions on Pattern Analysis and Machine Intelligence* **16**, 824–831.
- Oltmans SJ, Lefohn AS, Scheel HE, et al.** 1998. Trends of ozone in the troposphere. *Geophysical Research Letters* **25**, 139–142.
- Omasa K.** 2000. 3-D color video microscopy of intact plants. In: Häder DP, ed. *Image analysis: methods and applications*, 2nd edn. Boca Raton, FL: CRC Press, 257–273.
- Omasa K, Hashimoto Y, Aiga I.** 1981. A quantitative analysis of the relationships between O<sub>3</sub> sorption and its acute effects on plant leaves using image instrumentation. *Environmental Control in Biology* **19**, 85–92.
- Omasa K, Shimazaki K, Aiga I, Larcher W, Onoe M.** 1987. Image analysis of chlorophyll fluorescence transients for diagnosing the photosynthetic system of attached leaves. *Plant Physiology* **84**, 748–752.
- Omasa K, Tobe K, Hosomi M, Kobayashi M.** 2000. Absorption of ozone and seven organic pollutants by *Populus nigra* and *Camellia sasanqua*. *Environmental Science and Technology* **34**, 2498–2500.
- Omasa K, Tobe K, Kondo T.** 2002. Absorption of organic and inorganic air pollutants by plants. In: Omasa K. In: Saji H, Youssefian S, Kondo N, eds. *Air pollution and plant biotechnology: prospects for phytomonitoring and phytoremediation*. Tokyo: Springer-Verlag, 155–178.
- Oxborough K, Baker NR.** 1997. An instrument capable of imaging chlorophyll *a* fluorescence from intact leaves at very low irradiance and at cellular and subcellular levels of organization. *Plant, Cell and Environment* **20**, 1473–1483.
- Pell EJ, Eckhard N, Eniyedi AJ.** 1992. Timing of ozone stress and resulting status of ribulose biphosphate carboxylase-oxygenase and associated net photosynthesis. *New Phytologist* **120**, 397–408.
- Rolfe SA, Scholes JD.** 2002. Extended depth-of-focus imaging of chlorophyll fluorescence from intact leaves. *Photosynthesis Research* **72**, 107–115.
- Russ JC.** 1998. *The image processing handbook*, 3rd edn. London: CRC Press.
- Sandermann H, Wellburn AR, Heath RL.** 1997. *Forest decline and ozone*. Berlin: Springer-Verlag.
- Schraudner M, Langerbartels C, Sanderman H.** 1997. Changes in the biochemical status of plant cells induced by the environmental pollutant ozone. *Physiologia Plantarum* **100**, 274–280.
- Torsethaugen G, Pell EJ, Assmann SM.** 1999. Ozone inhibits guard cell K<sup>+</sup> channels implicated in stomatal opening. *Proceedings of the National Academy of Sciences, USA* **96**, 13577–13582.
- Yunus M, Iqbal M.** 1996. *Plant response to air pollution*. New York: John Wiley & Sons.